Applied Mathematics and Computation 258 (2015) 489–501

Contents lists available at ScienceDirect

Applied Mathematics and Computation

journal homepage: www.elsevier.com/locate/amc

Transient analysis of single-layered graphene sheet using the kp-Ritz method and nonlocal elasticity theory

Yang Zhang [a,b], L.W. Zhang [c,*], K.M. Liew [b,d], J.L. Yu [a]

[a] CAS Key Laboratory of Mechanical Behavior and Design of Materials, University of Science and Technology of China, Hefei, China
[b] Department of Architecture and Civil Engineering, City University of Hong Kong, Kowloon, Hong Kong Special Administrative Region
[c] College of Information Technology, Shanghai Ocean University, Shanghai 201306, China
[d] City University of Hong Kong Shenzhen Research Institute Building, Shenzhen Hi-Tech Industrial Park, Nanshan District, Shenzhen, China

ARTICLE INFO

Keywords:
Single-layered graphene sheets
Transient analysis
kp-Ritz method

ABSTRACT

In this paper, an investigation on the transient analysis of single-layered graphene sheets (SLGSs) is performed using the element-free kp-Ritz method. The classical plate theory is used to describe the dynamic behavior of SLGSs. Nonlocal elasticity theory, in which nonlocal parameter is introduced, is incorporated to reflect the small effect. Newmark's method is employed to solve the discretized dynamic equations. Several numerical examples are presented to examine the effect of boundary conditions, aspect ratio, side length load distribution type and load variation type on the transient behavior of SLGSs. The present work can serve as the foundation for further investigation of the transient response of multi-layered graphene sheets.

1. Introduction

Graphene consists of covalently bonded carbon atoms tightly packed in a honeycomb crystal lattice which is the most promising electromechanical material in the coming decades for miniaturization of electromechanical devices. It has outstanding mechanical, electrical and thermal properties. Its Young's modulus is approximately 1.0 TPa, electronic mobility limited to 2e + 5 $cm^2/(V\ s)$ and thermal conductivity of 3000 W/(m K) [1–4].

Graphene sheets (GSs) are the fundamental structural element of carbon structures such as graphite, carbon nanotubes (CNTs) and fullerenes, and thus, in order to better apply graphene sheet to nano-electromechanical systems (NEMSs), an adequate understanding of its mechanical properties is required to make the graphene-based electromechanical devices mechanically actuated precisely.

Extant literature has reported extensive investigations of mechanical properties of GSs. Atalaya et al. [5] studied both elastostatics and elastodynamics problems for square graphene-based resonators using nonlinear finite elasticity theory. Scarpa et al. [6] described linear elastic properties of GSs with truss-type analytical models. Linear and nonlinear vibrations of GSs were investigated based on nonlinear inter-atomic potential function by Sadeghi and Naghdabadi [7]. Arash et al. [8] analyzed the wave propagation characteristics of GSs using the nonlocal elastic plate model that accounts for the small scale effects. The elastic buckling behavior of defect-free GSs is investigated using an atomistic modeling approach [9]. An atomistic based finite element model considering large deformation and nonlinear geometric effects was derived by Baykasoglu

* Corresponding author.
E-mail address: lwzhang@shou.edu.cn (L.W. Zhang).

http://dx.doi.org/10.1016/j.amc.2015.02.023
0096-3003/

and Mugan [10] for prediction of fracture behavior of single-layer graphene sheets (SLGSs). Although there have been numerous studies of the above GS problems, less work seems to have been done on the transient analysis of GS. However, there is a need to have a good knowledge of the transient response of GS because many nano-electromechanical devices are subjected to dynamic loads. For instance, there exists an electrostatic force between the suspended graphene sheet and the substrate when the graphene based electromechanical resonator is undergoing electrical modulation [11]. It is a fundamental issue to study the transient response of single-layered graphene sheets (SLGSs) because that can provide the basis for further study of transient response of multi-layered graphene sheets (MLGSs) in which Van der Waals force and electromagnetic force are concerned.

Theoretical and computational tools are vital to predict mechanical properties of GSs because of limitations of physical or experimental measurements of nano-scale devices. In general, computational models of nano-scale structures are classified to three main categories: (a) atomistic modeling, including ab initio and classical molecular dynamics [12,13]; (b) hybrid atomistic-continuum mechanics approach [14–16]; and (c) continuum mechanics approach [17–20]. Among these approaches, atomistic approach requires vast computational resources and although hybrid atomistic-continuum mechanics approach is computationally feasible in many problems, including material failure, crack propagation, grain boundaries and dislocation, it is complex to deal with the interface or "handshake" region between atomistic subset and continuum subset. Simulating GSs with traditional structural members such as spring, truss, beam, shell and plate, continuum approach is computationally less expensive and generated results are in good agreement with those of the other two approaches [21,22]. It is worth noting that continuum approach should be modified so as to reflect the small-scale effect in nanostructures. The most successful modified continuum approach considering the small-scale effect is the nonlocal elasticity theory proposed by Eringen [23,24]. By assuming the stress at a given point to be a function of both the strain at that point and the strains at all other points in the domain, the nonlocal elasticity theory captures the small-scale effect successfully [17,18,25–30].

Many numerical techniques have been applied to investigate the properties of nanostructures, described by the continuum model. Pradhan and Kumar [31] employed the differential quadrature method to study vibration characteristics of orthotropic GSs. The finite element method was applied by Arash et al. [8] to simulate wave propagation of GSs. Wang et al. [32] used the finite difference method to solve the nonlinear equations for circular graphene bubbles. Demir et al. [33] applied the discrete singular convolution (DSC) technique to investigate the free vibration behavior of carbon nanotubes. The element-free kp-Ritz method was employed as an efficient numerical tool for analyzing mechanical properties of materials ranging from nano-scale to macro-sale [34–46]. It is worthy pointing out that the kp-Ritz method shares some common features with the DSC-Ritz method [47,48]; both are effective and efficiency numerical approaches for solving PDEs in engineering although they employed different mathematical foundations to construct their shape function. Based on the theory of distribution and wavelet approximation, the DSC-Ritz scheme was able to predict the missing vibration modes of the Kirchhoff–Mindlin plate relationship due to the lack of consideration for the transverse shear modes and the coupled bending–shear modes in the relationship [49].

In the present work, the nonlocal elasticity theory is adopted. The element-free kp-Ritz method is employed for the transient analysis of SLGSs by solving the governing equations derived from the classical plate theory incorporating the nonlocal elasticity theory. The dynamic equations are solved using the Newmark method. The effects of: (1) boundary conditions, (2) aspect ratios, (3) size of the SLGSs, (4) nonlocal parameter, and (5) load types on the non-dimensional transient response are studied. The present study will be useful for further investigation of the dynamic response of MLGSs and instructive to the design of nano-electromechanical devices.

2. Formulation with nonlocal elasticity theory

According to the Hamilton's principle, the dynamic behavior of SLGSs can be described as

$$\delta \int_{t_1}^{t_2} \left[K - (U_{strain} + V_{force})\right] dt = 0, \tag{1}$$

where the kinetic energy K, the strain energy U_{strain} and the external potential V_{force} are expressed using the classical plate theory (CPT) which assumes that the straight line remains straight and vertical to the mid-plane after deformation, despite the shear deformation and rotational inertia. According to the CPT, when the small deflection is assumed, the displacement can be expressed as

$$u(x, y, z; t) = -z\frac{\partial w}{\partial x}, \tag{2}$$

$$v(x, y, z; t) = -z\frac{\partial w}{\partial y}, \tag{3}$$

$$w(x, y, z; t) = w(x, y; t). \tag{4}$$

Subsequently, the strain–displacement relations can be obtained as

$$\varepsilon_{xx} = -z\frac{\partial^2 w}{\partial x^2}, \tag{5}$$

$$\varepsilon_{yy} = -z\frac{\partial^2 w}{\partial y^2}, \tag{6}$$

$$\varepsilon_{zz} = 0, \tag{7}$$

$$\gamma_{xy} = -2z\frac{\partial^2 w}{\partial xy}, \tag{8}$$

$$\gamma_{xz} = \gamma_{yz} = 0. \tag{9}$$

Thus, the strain energy can be expressed as

$$U_{strain} = \frac{1}{2}\int_{\Omega} \vec{\sigma}^T \cdot \vec{\varepsilon} d\Omega, \tag{10}$$

where $\vec{\sigma} = [\sigma_{xx,}\sigma_{yy}, \sigma_{xy}]^T$, $\vec{\varepsilon} = [\varepsilon_{xx,}\varepsilon_{yy}, \varepsilon_{xy}]^T$.

The external potential can be expressed as

$$V_{force} = \int_{\Omega} q \cdot w d\Omega, \tag{11}$$

where q is external force perpendicular to the surface of SLGSs and the kinetic energy can be written as

$$K = \frac{1}{2}\int_{\Omega} \rho\left[\left(-z\frac{\partial \dot{w}}{\partial x}\right)^2 + \left(-z\frac{\partial \dot{w}}{\partial y}\right) + \dot{w}^2\right] d\Omega. \tag{12}$$

Substituting Eqs. (10)–(12) into Eq. (1) leads to

$$M_{x,xx} + 2M_{xy,xy} + M_{yy,yy} + q = I_0 w_{,tt} - I_2(w_{,xxtt} + w_{,yytt}), \tag{13}$$

where $[M_{xx}, M_{xy}, M_{yy}]^{\mathrm{T}} = \int_{-\frac{h}{2}}^{\frac{h}{2}} [\sigma_{xx}, \sigma_{xy}, \sigma_{yy}]^{\mathrm{T}} z dz$, $[I_0, I_2]^{\mathrm{T}} = \int_{-\frac{h}{2}}^{\frac{h}{2}} [1, z^2]\rho_0 dz$. ρ_0 is the density of SLGSs.

The nonlocal elasticity theory accounts for small scale effect by assuming that the stress field at a reference point depends not only on strain at that point but also on strains at all other points of the domain. Thus, the constitutive relation of nonlocal elasticity theory contains an integral over the whole body in which nonlocal parameters are introduced to reflect the small scale effect. The other form of nonlocal constitutive relation is the differential constitutive, which is most widely used. According to [50], the differential form obtained from the integrated form can be written as:

$$\left(1 - (e_0 a)^2 \nabla^2\right)\sigma_{ij} = C_{ijkl} : \varepsilon_{kl}, \tag{14}$$

where $(e_0 a)^2$ denotes the non-local parameters, σ_{ij} is the non-local stress, e_0 is the nonlocal material constant ranging from 0 to 14 [51], a is internal characteristic lengths (such as length of C–C bonds, lattice parameter), C_{ijkl} and ε_{kl} are the local stiffness tensor and traditional strain, respectively.

The stress–strain relationship of the non-local plate can be described as

$$\begin{Bmatrix} \sigma_{xx} \\ \sigma_{yy} \\ \sigma_{xy} \end{Bmatrix} - (e_0 a)^2 \nabla^2 \begin{Bmatrix} \sigma_{xx} \\ \sigma_{yy} \\ \sigma_{xy} \end{Bmatrix} = \begin{bmatrix} E/(1-\upsilon^2) & \upsilon E/(1-\upsilon^2) & 0 \\ \upsilon E/(1-\upsilon^2) & E/(1-\upsilon^2) & 0 \\ 0 & 0 & G \end{bmatrix} \begin{bmatrix} \varepsilon_{xx} \\ \varepsilon_{yy} \\ \varepsilon_{xy} \end{bmatrix}, \tag{15}$$

where E, υ and G denote the elastic modulus, Poisson's ratio and shear modulus, respectively. Thus, the nonlocal moments can be expressed as

$$M_{xx} - (e_0 a)^2 \nabla^2 M_{xx} = -D\left(\frac{\partial^2 w}{\partial x^2} + \upsilon\frac{\partial^2 w}{\partial y^2}\right), \tag{16}$$

$$M_{yy} - (e_0 a)^2 \nabla^2 M_{yy} = -D\left(\frac{\partial^2 w}{\partial y^2} + \upsilon\frac{\partial^2 w}{\partial x^2}\right), \tag{17}$$

$$M_{xy} - (e_0 a)^2 \nabla^2 M_{xy} = -D(1-\upsilon)\frac{\partial^2 w}{\partial x \partial y}. \tag{18}$$

Substituting Eqs. (16)–(18) into Eq. (13), the following governing equation for the problem can be obtained

$$-D\nabla^4 w = \left[1-(e_0a)^2\nabla^2\right]\left[I_0 w_{,tt} - I_2(w_{,xxtt}+w_{,yytt}) - q\right], \tag{19}$$

where $D = Eh^3/12(1-v^2)$ is the bending rigidity of the SLGSs while E, h and v are Young's modulus, thickness and Poisson's ratio, respectively.

3. Element-free kp-Ritz method and discretized matrix equation

3.1. Element-free kp-Ritz method

The discretized generic displacement field can be expressed as

$$w = \sum_{I=1}^{NP}\psi_I(\boldsymbol{x})w_I, \tag{20}$$

where $\psi_I(\boldsymbol{x})$ and w_I are the shape function and nodal parameter, respectively, and NP is the number of distributed nodes. Based on reproducing kernel particle method [52,53], the shape functions can be defined as

$$\psi_I(\boldsymbol{x}) = C(\boldsymbol{x};\boldsymbol{x}-\boldsymbol{x}_I)\Phi_a(\boldsymbol{x}-\boldsymbol{x}_I), \tag{21}$$

where $\Phi_a(\boldsymbol{x}-\boldsymbol{x}_I)$ is the kernel function and $C(\boldsymbol{x};\boldsymbol{x}-\boldsymbol{x}_I)$ is the correction function which satisfies reproducing conditions

$$\sum_{I=1}^{NP}\psi_I(\boldsymbol{x})x_I^p y_I^q = x^p y^q \quad \text{for} \quad p+q = 0,1,2, \tag{22}$$

$$C(\boldsymbol{x};\boldsymbol{x}-\boldsymbol{x}_I) = \mathbf{H}^{\mathrm{T}}(\boldsymbol{x}-\boldsymbol{x}_I)\mathbf{b}(\boldsymbol{x}), \tag{23}$$

where

$$\mathbf{b}(\boldsymbol{x}) = [b_0(x,y), b_1(x,y), b_2(x,y), b_3(x,y), b_4(x,y), b_5(x,y)]^{\mathrm{T}}, \tag{24}$$

$$\mathbf{H}^{\mathrm{T}}(\boldsymbol{x}-\boldsymbol{x}_I) = [1, x-x_I, y-y_I, (x-x_I)(y-y_I), (x-x_I)^2, (y-y_I)^2]. \tag{25}$$

The shape function is written as

$$\psi_I(\boldsymbol{x}) = \mathbf{b}^{\mathrm{T}}(\boldsymbol{x})\mathbf{H}(\boldsymbol{x}-\boldsymbol{x}_I)\Phi_a(\boldsymbol{x}-\boldsymbol{x}_I). \tag{26}$$

Substituting Eq. (20) into Eq. (22) leads to

$$\mathbf{b}(\boldsymbol{x}) = \mathbf{M}^{-1}(\boldsymbol{x})\mathbf{H}(\mathbf{0}), \tag{27}$$

where

$$\mathbf{M}(\boldsymbol{x}) = \sum_{I=1}^{NP}\mathbf{H}(\boldsymbol{x}-\boldsymbol{x}_I)\mathbf{H}^{\mathrm{T}}(\boldsymbol{x}-\boldsymbol{x}_I)\Phi_a(\boldsymbol{x}-\boldsymbol{x}_I), \tag{28}$$

$$\mathbf{H}(\mathbf{0}) = [1,0,0,0,0,0,]^{\mathrm{T}}, \tag{29}$$

and $\Phi_a(\boldsymbol{x}-\boldsymbol{x}_I)$ is defined as follow

$$\Phi_a(\boldsymbol{x}-\boldsymbol{x}_I) = \Phi_a(x)\cdot\Phi_a(y), \tag{30}$$

where

$$\Phi_a(x) = \varphi\left(\frac{x-x_I}{a}\right). \tag{31}$$

The cubic spline function is adopted as the weight function $\varphi(x)$

$$\varphi_z(z_I) = \begin{Bmatrix} \frac{2}{3}-4z_I^2+4z_I^3 & \text{for} \quad 0\leqslant|z_I|\leqslant\frac{1}{2} \\ \frac{4}{3}-4z_I+4z_I^2-\frac{4}{3}z_I^3 & \text{for} \quad \frac{1}{2}<|z_I|\leqslant 1 \\ 0 & \text{otherwise} \end{Bmatrix}, \tag{32}$$

where

$$Z_I = \frac{x-x_I}{d_I}, \tag{33}$$

$$d_I = d_{\max}c_I, \tag{34}$$

in which d_I is the size of the support, $d_{\max}$ is a scaling factor and distance c_I is chosen by searching a sufficient number of nodes to avoid the singularity of matrix $\mathbf{M}$.

Thus, the shape function is obtained as

$$\psi_I(\boldsymbol{x}) = \mathbf{H}^{\mathrm{T}}(\mathbf{0})\mathbf{M}^{-1}(\boldsymbol{x})\mathbf{H}(\boldsymbol{x}-\boldsymbol{x}_I)\Phi_a(\boldsymbol{x}-\boldsymbol{x}_I). \tag{35}$$

Since the present shape function $\psi_I(\boldsymbol{x})$ does not possess the Kronecker delta property, the transformation method [54] is applied to impose the essential boundary conditions. For the transformation approach, a transformation matrix is developed for reconstruction of the present shape functions that have the Kronecker delta property.

3.2. Weak form of governing equation

When the original strong form equilibrium equation is multiplied by the virtual displacement δw, the following equation is obtained:

$$\int_\Omega \delta w\left\{D\nabla^4 w + \left[1-(e_0a)^2\nabla^2\right]\left[I_0 w_{,tt} - I_2(w_{,xxtt}+w_{,yytt}) - q\right]\right\}dxdy = 0. \tag{36}$$

The above equation can then be integrated by part as:

$$\begin{aligned}
&\int_\Omega D(\delta w_{,xx}w_{,xx} + 2\delta w_{,xy}w_{,xy} + \delta w_{,yy}w_{,yy})dxdy + \int_\Omega (I_0\delta w w_{,tt} + I_2(\delta w_{,x}w_{,xtt} + \delta w_{,y}w_{,ytt}))dxdy \\
&\quad + (e_0a)^2\int_\Omega (I_0(\delta w_{,x}w_{,xtt} + \delta w_{,y}w_{,ytt}) + I_2(\delta w_{,xx}w_{,xxtt} + 2\delta w_{,xy}w_{,xytt} + \delta w_{,yy}w_{,yytt}))dxdy \\
&\quad - \int_\Omega \delta w q dxdy + (e_0a)^2\int_\Omega \delta w(q_{,xx}+q_{,yy})dxdy + \int_\Gamma D(\delta w w_{,xxx}n_x - \delta w_{,x}w_{,xx}n_x + 2\delta w w_{,xyy}n_x \\
&\quad - 2\delta w_{,x}w_{,xy}n_y + \delta w w_{,yyy}n_y - \delta w_{,y}w_{,yy}n_y)ds - \int_\Gamma (I_2 + (e_0a)^2 I_0)(\delta w w_{,xtt}n_x + \delta w w_{,ytt}n_y)ds \\
&\quad + (e_0a)^2\int_\Gamma I_2((\delta w w_{,xxxtt} - \delta w_{,x}w_{,xxtt})(n_x+n_y) + 2\delta w w_{,xyytt}n_x + 2\delta w_{,x}w_{,xytt}n_y)ds = 0.
\end{aligned} \tag{37}$$

3.3. Discretized algebraic equations

Substituting Eq. (20) into Eq. (37), the discretized algebraic equations can be obtained as

$$\boldsymbol{M}\ddot{\boldsymbol{W}}(t) + \boldsymbol{K}\boldsymbol{W}(t) = \boldsymbol{F}(t), \tag{38}$$

where

$$[\boldsymbol{M}] = [M_L] + [M_{NL}], \tag{39}$$

$$[M_L] = \int_\Omega [N_L]^T G_L [N_L] d\Omega, \quad [M_{NL}] = \int_\Omega (e_0a)^2 [N_{NL}]^T G_{NL}[N_{NL}]d\Omega, \tag{40}$$

$$[N_L(I)] = \begin{bmatrix} \Psi_I \\ \Psi_{I,x} \\ \Psi_{I,y} \end{bmatrix}, \quad G_L = \begin{bmatrix} I_0 & 0 & 0 \\ 0 & I_2 & 0 \\ 0 & 0 & I_2 \end{bmatrix}, \tag{41}$$

$$[N_{NL}(I)] = \begin{bmatrix} \Psi_{I,x} \\ \Psi_{I,y} \\ \Psi_{I,xx} \\ \Psi_{I,xy} \\ \Psi_{I,yy} \end{bmatrix}, \quad G_{NL} = \begin{bmatrix} I_0 & 0 & 0 & 0 & 0 \\ 0 & I_0 & 0 & 0 & 0 \\ 0 & 0 & I_2 & 0 & 0 \\ 0 & 0 & 0 & 2I_2 & 0 \\ 0 & 0 & 0 & 0 & I_2 \end{bmatrix}, \tag{42}$$

$$[\boldsymbol{K}] = \int_\Omega [B]^T R[B]d\Omega, \tag{43}$$

$$B(I) = \begin{bmatrix} \Psi_{I,xx} \\ \Psi_{I,xy} \\ \Psi_{I,yy} \end{bmatrix}^T, \quad R = diag\{D, 2D, D\}. \tag{44}$$

4. Numerical results and discussion

The appropriate value of the scaling factor can be calibrated through comparison of power spectral density properties of transient response with modal features of SLGSs. For this purpose, the transient response of square SLGSs with side length of 10 nm is simulated. The dynamic deflection of central point is studied to show the dynamic characteristics of SLGSs, which is under transverse sudden load distributed uniformly with the value of 1.0*e*4 N/m^2. According to [55], mechanical parameters of the SLGSs are taken as: the Young's modulus E = 1.02 TPa, the Poisson's ratio v = 0.16, the mass density $\rho = 2250$ kg/m^3 and the thickness h = 0.34 nm. The fundamental frequency of square SLGSs with side length of 10 nm is 69.1 GHz. It is simply supported in all four edges (SSSS). Fig. 1 shows the power spectral density properties of transient response of square SLGSs with side length of 10 nm. It indicates that the fundamental frequency of SLGSs is 66.4 GHz, which coincides with that of [55]. Fig. 2 illustrates the power spectral density properties of transient response of SLGSs with the same size. It is clamped in all four edges (CCCC). It can be found that the fundamental frequency of SLGSs is 127 GHz, which is close to the result of [27]. Thus, the scaling factor can be determined, which equals 2.3. In the following simulations, the nondimensional deflection is defined by [56] as

$$\bar{w} = w \times \frac{Eh^3}{qb^4} \times 10^2, \tag{45}$$

where b denotes the width of SLGSs.

To examine the influence of boundary conditions on the transient response of SLGSs, the dynamic behavior of square SLGSs with side length of 10 nm under uniformly distributed transverse sudden load was simulated. Three kinds of boundary conditions were considered: (a) simply supported in all four edges (SSSS); (b) clamped in all four edges (CCCC); and (c) simply supported in two opposite edges and clamped in the other two opposite edges (CSCS). The variation of nondimensional

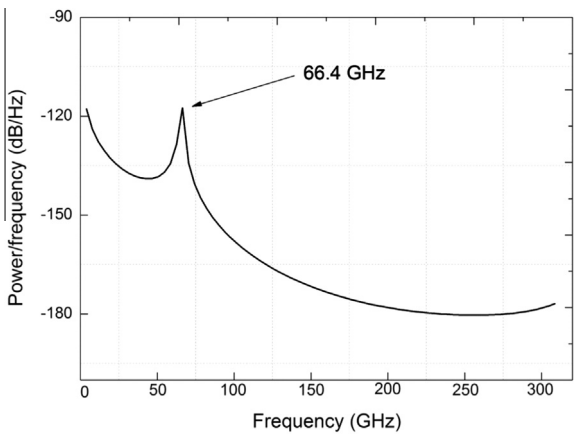

Fig. 1. Power spectrum density plot of SLGS subjected to SSSS boundary conditions.

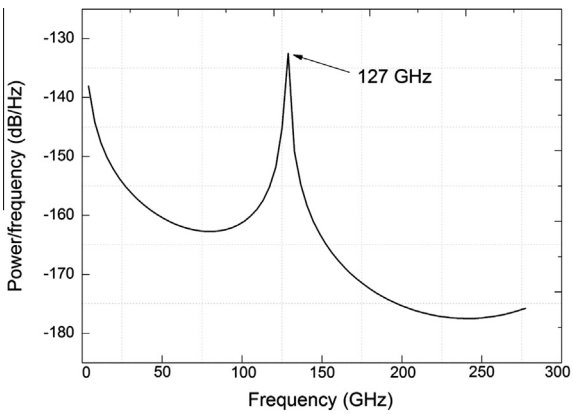

Fig. 2. Power spectrum density plot of SLGS subjected to CCCC boundary conditions.

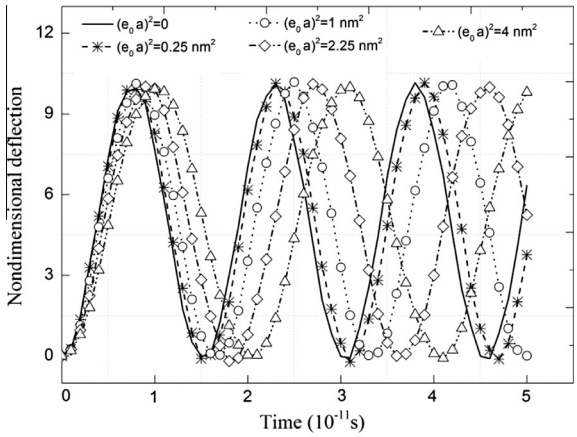

Fig. 3. Variation of nondimensional displacement of center point of SLGSs subjected to SSSS boundary conditions for different nonlocal parameters.

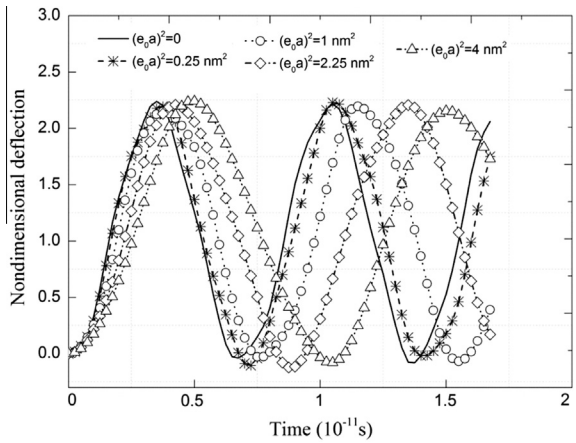

Fig. 4. Variation of nondimensional displacement of center point of SLGSs subjected to CCCC boundary conditions for different nonlocal parameters.

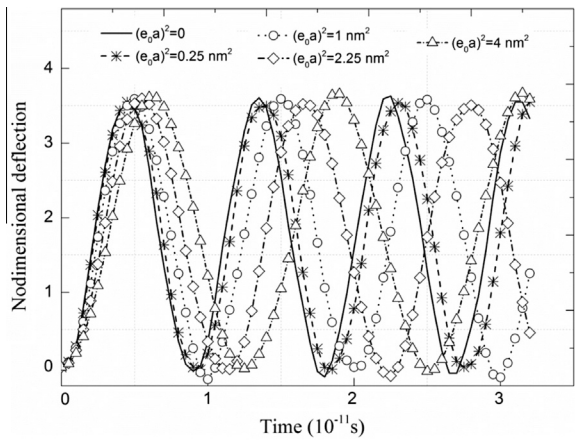

Fig. 5. Variation of nondimensional displacement of center point of SLGSs subjected to CSCS boundary conditions for different nonlocal parameters.

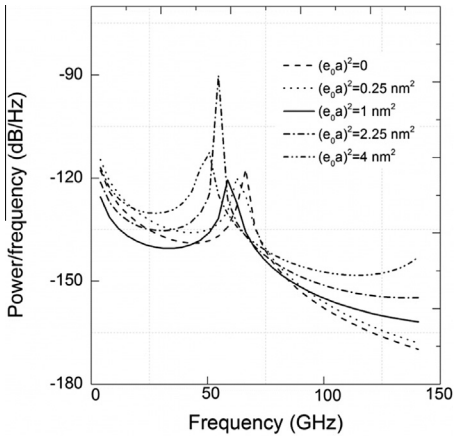

Fig. 6. Power spectrum density plot of SLGS subjected to SSSS boundary conditions for different nonlocal parameters.

displacement of center point of SLGSs subjected to SSSS, CCCC, CSCS boundary conditions for different nonlocal parameters is plotted in Figs. 3–5, respectively. The power spectral density properties of the transient response of square SLGSs corresponding to various nonlocal parameters are plotted in Fig. 6. It is observed from Figs. 3–5 that an increase in nonlocal parameters causes an increase of the period of vibration. In other words, as nonlocal parameters increase, the frequency of vibration decreases. This indicates that SLGSs tend to be softer when nonlocal effect is concerned. The same conclusion can be drawn from Fig. 6. It can be seen from the comparison of nondimensional amplitude in Figs. 3–5 that the rank of fastening effects of different boundary conditions is CCCC, CSCS and SSSS.

The effect of aspect ratio on the transient behavior of SLGSs is investigated by simulating the dynamic response of SLGSs with constant width of 10 nm subjected to SSSS boundary conditions under uniformly distributed transverse sudden load. The expression of aspect ratio is written as

$$aspect\ ratio = \frac{length}{width}.$$

Fig. 7 depicts the variation of nondimensional displacement of center point of SLGSs vs. time for different aspect ratios. In Fig. 8, the power spectral density properties of transient response of square SLGSs for different aspect ratios are plotted. From Figs. 7 and 8, we can draw a conclusion that the increase of aspect ratio causes the increase of amplitude and period of dynamic vibration.

The variation of nondimensional displacement of center point of SLGSs vs. time for different side lengths is depicted in Fig. 9. The power spectral density properties of transient response of square SLGSs for different side lengths are presented in Fig. 10. Herein, square SLGSs with different side lengths subjected to SSSS boundary conditions under uniformly distributed transverse sudden load are simulated. The nonlocal parameter is set to be 0. Five side lengths, 10 nm, 15 nm, 20 nm, 25 nm and 30nm are considered. Figs. 9 and 10 show that the vibration period increases with increase of side length.

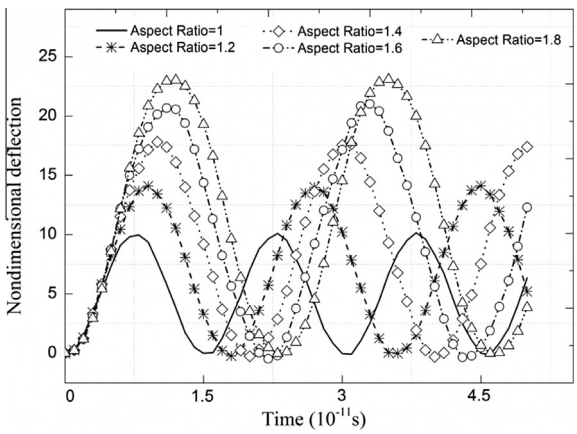

Fig. 7. Variation of nondimensional displacement of center point of SLGSs vs. time for different aspect ratios.

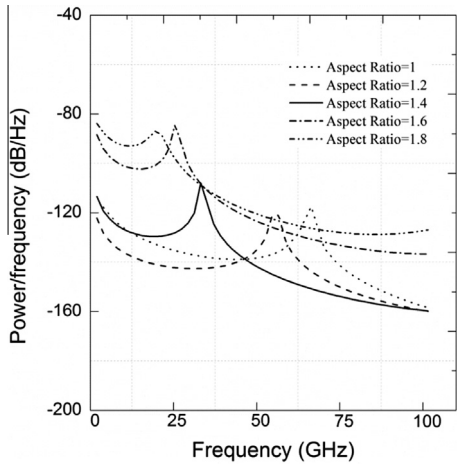

Fig. 8. Power spectrum density plot of SLGS subjected to SSSS boundary conditions for different aspect ratios.

To investigate the influence of load type on dynamic response of SLGSs, two load types (i.e., load type I and load type II) are simulated. Load type I is uniformly distributed load containing four cases according to different load distribution areas, as illustrated in Fig. 11: (1) Load type I-1 [0-1/4]; (2) Load type I-2 [1/4-1/2]; (3) Load type I-3 [0-1/2]; and (4) Load type I-4 [1/4-3/4]. The value of such uniformly distributed load is $1e4\ \mathrm{N/m^2}$. Load type II is variable along x axis instead of uniform distribution, one of which named Load type II-1 has the following expression

$$q = \lambda q_0 + q_0 \sin(kx). \tag{46}$$

In the present study, three cases are considered (Figs. 12–14):

(1) $\lambda = 0,\ q_0 = 1e4\ \mathrm{N/m^2},\ k = 1e3;$
(2) $\lambda = 1,\ q_0 = 1e4\ \mathrm{N/m^2},\ k = 1e3;$
(3) $\lambda = 1,\ q_0 = 1e4\ \mathrm{N/m^2},\ k = 5e9.$

Load type II-2 has the following formula

$$q = q_0 e^{kx}, \tag{47}$$

In this situation, two cases are considered (Figs. 15 and 16):

(1) $q_0 = 1e4\ \mathrm{N/m^2},\ k = 1e3;$
(2) $q_0 = 1e4\ \mathrm{N/m^2},\ k = 5e8.$

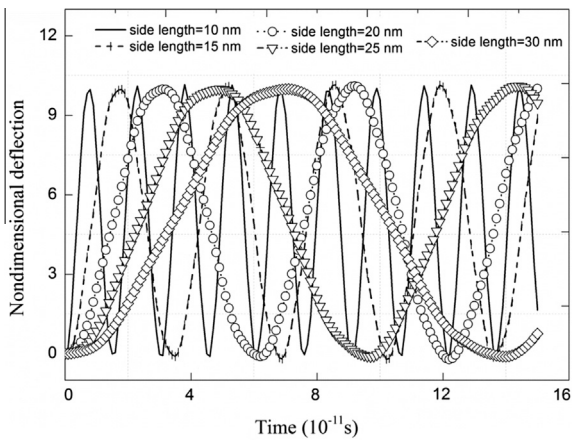

Fig. 9. Variation of nondimensional displacement of center point of SLGSs vs. time for different side lengths.

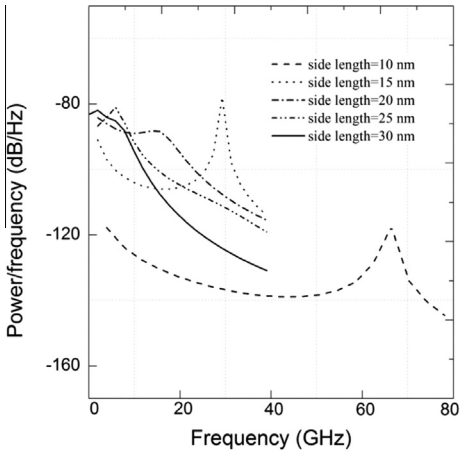

Fig. 10. Power spectrum density plot of SLGS subjected to SSSS boundary conditions for different side lengths.

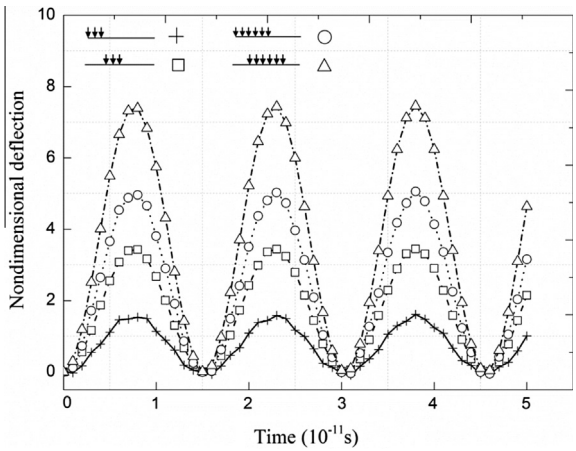

Fig. 11. Variation of nondimensional displacement of center point of SLGSs vs. time for different load distribution types (load type I).

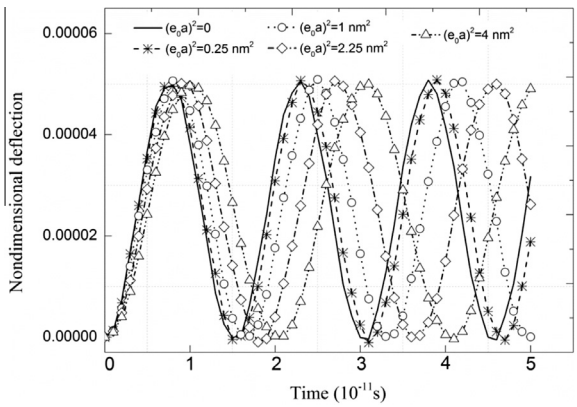

Fig. 12. Variation of nondimensional displacement of center point of SLGSs for different nonlocal parameters (load type II-1, $\lambda = 0, q_0 = 1e4\ \mathrm{N/m^2},\ k = 1e3$).

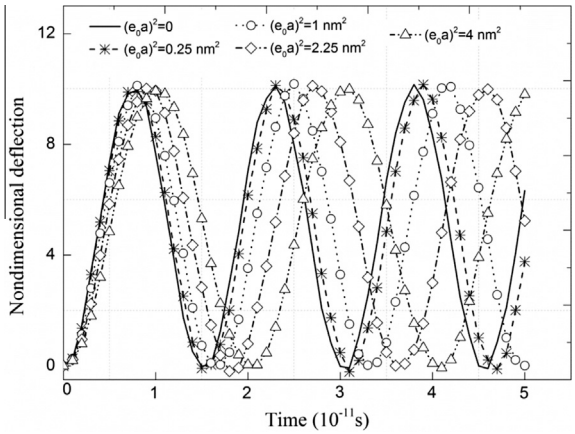

Fig. 13. Variation of nondimensional displacement of center point of SLGSs for different nonlocal parameters (load type II-1, $\lambda = 1, q_0 = 1e4\ \mathrm{N/m^2},\ k = 1e3$).

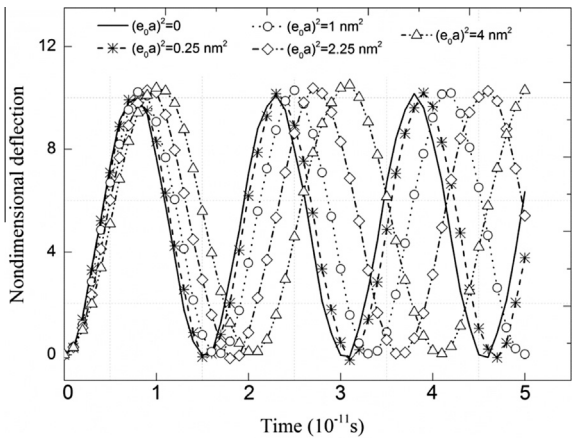

Fig. 14. Variation of nondimensional displacement of center point of SLGSs for different nonlocal parameters (load type II-1, $\lambda = 1, q_0 = 1e4\ \mathrm{N/m^2},\ k = 5e9$).

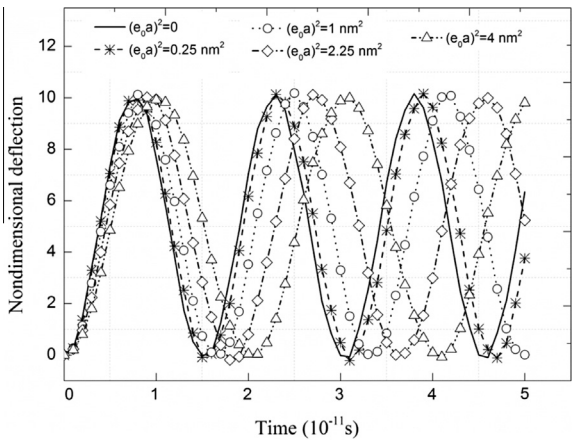

Fig. 15. Variation of nondimensional displacement of center point of SLGSs for different nonlocal parameters (load types II-2, $q_0 = 1e4\ \mathrm{N/m^2},\ k = 1e3$).

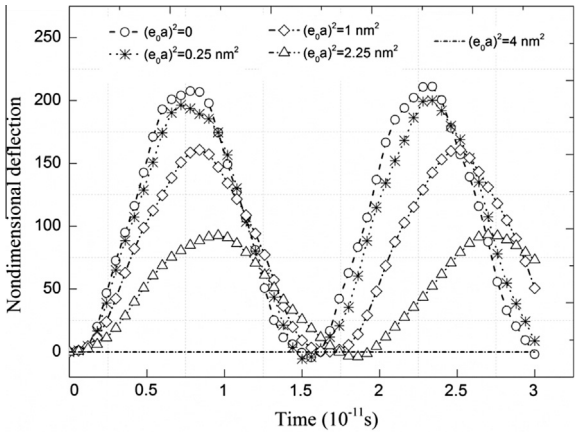

Fig. 16. Variation of nondimensional displacement of center point of SLGSs for different nonlocal parameters (load type II-2, $q_0 = 1e4\ \mathrm{N/m^2},\ k = 5e8$).

The dynamic behavior of square SLGSs with side length of 10 nm subjected to SSSS boundary conditions is analyzed to study the influence of load type on the transient response. From Fig. 11, it can be found that the amplitude for load type I-3 and load type I-4 is larger than that for load type I-1 and load type I-2. This is because the applied area for the former two load types is larger than that for the latter two load types. The reason why the amplitude for load type I-4 is larger than that for load type I-3 and the amplitude for load type I-2 is larger than that for load type I-1 is that the applied area for load type I-4 and load type I-2 is closer to the center of SLGSs. However, such load type has no influence on the vibration period of SLGSs. For load type II-1, the dynamic responses for three cases are plotted in Figs. 12–14. It can be seen that nonlocal parameter has slight impact on the vibration period of SLGS. However, it has evident influence on the amplitude of vibration. In contrast, for load type II-2, nonlocal parameter has influence on both the vibration period and amplitude of SLGSs. It is worth noting that in such load type, the wave number k has important influence on transient response of SLGSs. Fig. 16 shows that when k is large, it has significant effect on the amplitude of vibration. It can also be observed that the wave number has no influence on the vibration period of SLGSs.

5. Conclusion

In this paper, elastodynamic analysis of SLGSs subjected to a transverse sudden dynamic load is presented, for different boundary conditions, nonlocal parameters, aspect ratio, side length and load types. Classical plate theory is employed to describe the dynamic behavior of SLGSs. Nonlocal elasticity theory is incorporated to capture the small scale effect. The governing partial differential equation is solved by the element-free kp-Ritz method. The time-differencing is performed through the Newmark method. One interesting phenomenon observed is that the wave number for load type II-2 has significant influence on the vibration amplitude of SLGSs when it is large enough.

Acknowledgements

The work described in this paper was fully supported by grants from the Research Grants Council of the Hong Kong Special Administrative Region, China (Project No. 9042047, CityU 11208914) and the National Natural Science Foundation of China (Grant Nos. 11402142 and 51378448).

References

[1] C. Gómez-Navarro, R.T. Weitz, A.M. Bittner, M. Scolari, A. Mews, M. Burghard, K. Kern, Electronic transport properties of individual chemically reduced graphene oxide sheets, Nano Lett. 7 (2007) 3499–3503.
[2] C. Lee, X. Wei, J.W. Kysar, J. Hone, Measurement of the elastic properties and intrinsic strength of monolayer graphene, Science 321 (2008) 385–388.
[3] S. Stankovich, D.A. Dikin, G.H.B. Dommett, K.M. Kohlhaas, E.J. Zimney, E.A. Stach, R.D. Piner, S.T. Nguyen, R.S. Ruoff, Graphene-based composite materials, Nature 442 (2006) 282–286.
[4] A.H. Castro Neto, F. Guinea, N.M.R. Peres, K.S. Novoselov, A.K. Geim, The electronic properties of graphene, Rev. Mod. Phys. 81 (2009) 109–162.
[5] J. Atalaya, A. Isacsson, J.M. Kinaret, Continuum elastic modeling of graphene resonators, Nano Lett. 8 (2008) 4196–4200.
[6] F. Scarpa, S. Adhikari, A.S. Phani, Effective elastic mechanical properties of single layer graphene sheets, Nanotechnology 20 (2009) 065709.
[7] M. Sadeghi, R. Naghdabadi, Nonlinear vibrational analysis of single-layer graphene sheets, Nanotechnology 21 (2010) 105705.
[8] B. Arash, Q. Wang, K.M. Liew, Wave propagation in graphene sheets with nonlocal elastic theory via finite element formulation, Comput. Methods Appl. Mech. Eng. 223–224 (2012) 1–9.
[9] A. Sakhaee-Pour, Elastic buckling of single-layered graphene sheet, Comput. Mater. Sci. 45 (2009) 266–270.
[10] C. Baykasoglu, A. Mugan, Nonlinear fracture analysis of single-layer graphene sheets, Eng. Fract. Mech. 96 (2012) 241–250.
[11] J.S. Bunch, A.M. van der Zande, S.S. Verbridge, I.W. Frank, D.M. Tanenbaum, J.M. Parpia, H.G. Craighead, P.L. McEuen, Electromechanical resonators from graphene sheets, Science 315 (2007) 490–493.

[12] P. Ball, Roll up for the revolution, Nature 414 (2001) 142–144.
[13] R.H. Baughman, A.A. Zakhidov, W.A. de Heer, Carbon nanotubes-the route toward applications, Science 297 (2002) 787–792.
[14] B.H. Bodily, C.T. Sun, Structural and equivalent continuum properties of single-walled carbon nanotubes, Int. J. Mater. Prod. Technol. 18 (2003) 381–397.
[15] C. Li, T.W. Chou, A structural mechanics approach for the analysis of carbon nanotubes, Int. J. Solids Struct. 40 (2003) 2487–2499.
[16] C. Li, T.W. Chou, Single-walled carbon nanotubes as ultrahigh frequency nanomechanical resonators, Phys. Rev. B 68 (2003) 073405.
[17] J.N. Reddy, S.D. Pang, Nonlocal continuum theories of beams for the analysis of carbon nanotubes, J. Appl. Phys. 103 (2008) 023511.
[18] L. Shen, H.S. Shen, C.L. Zhang, Nonlocal plate model for nonlinear vibration of single layer graphene sheets in thermal environments, Comput. Mater. Sci. 48 (2010) 680–685.
[19] G.M. Odegard, T.S. Gates, L.M. Nicholson, K.E. Wise, Equivalent-continuum modeling of nano-structured materials, Compos. Sci. Technol. 62 (2002) 1869–1880.
[20] T. Murmu, S.C. Pradhan, Small-scale effect on the free in-plane vibration of nanoplates by nonlocal continuum model, Physica E 41 (2009) 1628–1633.
[21] C.M. Wang, V.B.C. Tan, Y.Y. Zhang, Timoshenko beam model for vibration analysis of multi-walled carbon nanotubes, J. Sound Vib. 294 (2006) 1060–1072.
[22] Q. Wang, V.K. Varadan, Wave characteristics of carbon nanotubes, Int. J. Solids Struct. 43 (2006) 254–265.
[23] A.C. Eringen, On differential equations of nonlocal elasticity and solutions of screw dislocation and surface waves, J. Appl. Phys. 54 (1983) 4703–4710.
[24] A.C. Eringen, Nonlocal Continuum Field Theories, Springer, New York, NY, USA, 2002.
[25] H. Babaei, A.R. Shahidi, Vibration of quadrilateral embedded multilayered graphene sheets based on nonlocal continuum models using the Galerkin method, Acta Mech. Sin. 27 (2011) 967–976.
[26] R. Ansari, R. Rajabiehfard, B. Arash, Nonlocal finite element model for vibrations of embedded multi-layered graphene sheets, Comput. Mater. Sci. 49 (2010) 831–838.
[27] R. Ansari, S. Sahmani, B. Arash, Nonlocal plate model for free vibrations of single-layered graphene sheets, Phys. Lett. A 375 (2010) 53–62.
[28] J.N. Reddy, Nonlocal nonlinear formulations for bending of classical and shear deformation theories of beams and plates, Int. J. Eng. Sci. 48 (2010) 1507–1518.
[29] H.S. Shen, Nonlocal shear deformable shell model for bending buckling of microtubules embedded in an elastic medium, Phys. Lett. A 374 (2010) 4030–4039.
[30] T. Murmu, S. Adhikari, Nonlocal mass nanosensors based on vibrating monolayer graphene sheets, Sens. Actuators B: Chem. 188 (2013) 1319–1327.
[31] S.C. Pradhan, A. Kumar, Vibration analysis of orthotropic graphene sheets using nonlocal elasticity theory and differential quadrature method, Compos. Struct. 93 (2011) 774–779.
[32] P. Wang, W. Gao, Z. Cao, K.M. Liechti, R. Huang, Numerical analysis of circular graphene bubbles, J. Appl. Mech. 80 (2013) 040905.
[33] C. Demir, O. Civalek, B. Akgoz, Free vibration analysis of carbon nanotubes based on shear deformable beam theory by discrete singular convolution technique, Math. Comput. Appl. 15 (2010) 57–65.
[34] K.M. Liew, X.Q. He, S. Kitipornchai, Predicting nanovibration of multi-layered graphene sheets embedded in an elastic matrix, Acta Mater. 54 (2006) 4229–4236.
[35] J.W. Yan, K.M. Liew, L.H. He, Predicting mechanical properties of single-walled carbon nanocones using a higher-order gradient continuum computational framework, Compos. Struct. 94 (2012) 3271–3277.
[36] J.W. Yan, K.M. Liew, L.H. He, Analysis of single-walled carbon nanotubes using the moving Kriging interpolation, Comput. Methods Appl. Mech. Eng. 229 (2012) 56–67.
[37] Z.X. Lei, K.M. Liew, J.L. Yu, Free vibration analysis of functionally graded carbon nanotube-reinforced composite plates using the element-free kp-Ritz method in thermal environment, Compos. Struct. 106 (2013) 128–138.
[38] Z.X. Lei, K.M. Liew, J.L. Yu, Buckling analysis of functionally graded carbon nanotube-reinforced composite plates using the element-free kp-Ritz method, Compos. Struct. 98 (2013) 160–168.
[39] Z.X. Lei, K.M. Liew, J.L. Yu, Large deflection analysis of functionally graded carbon nanotube-reinforced composite plates by the element-free kp-Ritz method, Comput. Methods Appl. Mech. Eng. 256 (2013) 189–199.
[40] Z.X. Lei, L.W. Zhang, K.M. Liew, J.L. Yu, Dynamic stability analysis of carbon nanotube-reinforced functionally graded cylindrical panels using the element-free kp-Ritz method, Compos. Struct. 113 (2014) 328–338.
[41] K.M. Liew, Z.X. Lei, J.L. Yu, L.W. Zhang, Postbuckling of carbon nanotube-reinforced functionally graded cylindrical panels under axial compression using a meshless approach, Comput. Methods Appl. Mech. Eng. 268 (2014) 1–17.
[42] J.W. Yan, L.W. Zhang, K.M. Liew, L.H. He, A higher-order gradient theory for modeling of the vibration behavior of single-wall carbon nanocones, Appl. Math. Model. 38 (2014) 2946–2960.
[43] L.W. Zhang, Y.J. Deng, K.M. Liew, An improved element-free Galerkin method for numerical modeling of the biological population problems, Eng. Anal. Boundary Elem. 40 (2014) 181–188.
[44] L.W. Zhang, Z.X. Lei, K.M. Liew, J.L. Yu, Large deflection geometrically nonlinear analysis of carbon nanotube-reinforced functionally graded cylindrical panels, Comput. Methods Appl. Mech. Eng. 273 (2014) 1–18.
[45] L.W. Zhang, Z.X. Lei, K.M. Liew, J.L. Yu, Static and dynamic of carbon nanotube reinforced functionally graded cylindrical panels, Compos. Struct. 111 (2014) 205–212.
[46] L.W. Zhang, P. Zhu, K.M. Liew, Thermal buckling of functionally graded plates using a local Kriging meshless method, Compos. Struct. 108 (2014) 472–492.
[47] C.W. Lim, Z.R. Li, G.W. Wei, DSC-Ritz method for high-mode frequency analysis of thick shallow shells, Int. J. Numer. Methods Eng. 62 (2005) 205–232.
[48] Y. Hou, G.W. Wei, Y. Xiang, DSC-Ritz method for the free vibration analysis of Mindlin plates, Int. J. Numer. Methods Eng. 62 (2005) 262–288.
[49] C.W. Lim, Z.R. Li, Y. Xiang, G.W. Wei, C.M. Wang, On the missing modes when using the exact frequency relationship between Kirchhoff and Mindlin plates, Adv. Vib. Eng. 4 (2005) 221–248.
[50] S. Sarrami-Foroushani, M. Azhari, Nonlocal vibration and buckling analysis of single and multi-layered graphene sheets using finite strip method including van der Waals effects, Physica E 57 (2014) 83–95.
[51] T. Murmu, S.C. Pradhan, Buckling analysis of a single-walled carbon nanotube embedded in an elastic medium based on nonlocal elasticity and Timoshenko beam theory and using DQM, Physica E 41 (2009) 1232–1239.
[52] W.K. Liu, S. Jun, Y.F. Zhang, Reproducing kernel particle methods, Int. J. Numer. Methods Fluids 20 (1995) 1081–1106.
[53] J.S. Chen, C. Pan, C.T. Wu, W.K. Liu, Reproducing Kernel particle methods for large deformation analysis of non-linear structures, Comput. Methods Appl. Mech. Eng. 139 (1996) 195–227.
[54] K.M. Liew, Y. Cheng, S. Kitipornchai, Boundary element-free method (BEFM) for two-dimensional elastodynamic analysis using Laplace transform, Int. J. Numer. Methods Eng. 64 (2005) 1610–1627.
[55] J.B. Wang, M.L. Tian, X.Q. He, Z.B. Tang, Free vibration analysis of single-layered graphene sheets based on a continuum model, Appl. Phys. Front. 2 (2014) 1–7.
[56] W.Y. Jung, S.C. Han, Nonlocal elasticity theory for transient analysis of higher-order shear deformable nanoscale plates, J. Nanomaterials 2014 (2014). 1–1.